ORIGINAL PAPER

EFFECT OF TEMPERATURE ON TITANIUM HYDRIDING KINETICS STUDIED BY THERMOGRAVIMETRY, FOR HYDROGEN ISOTOPES STORAGE

IRINA STURZEANU[1,2], MARIEA DEACONU[1], MARIOARA ABRUDEANU[2]

Manuscript received: 15.01.2026; Accepted paper: 06.05.2026;
Published online: 30.06.2026.

Abstract. *In the context of increasing demands for efficient hydrogen isotope storage in nuclear and non-nuclear energy applications, metal hydrides have gained significant attention as safe and viable storage methods. Their reversible absorption capability, high volumetric storage density, and stability under radiation exposure make them suitable candidates for advanced energy systems. However, the practical use of metal hydrides is often constrained by the kinetics of hydrogen absorption and desorption processes, which play a decisive role in material performance. Titanium is a promising hydrogen-storage material owing to its low density and high affinity for hydrogen, which enables the formation of stable, reversible metal hydrides. This study investigates the hydrogenation kinetics of Ti powder and determines the activation energy of the hydriding process using thermogravimetric analysis data and an Arrhenius plot. Ti powder was activated at 800 °C under Ar and subsequently hydrogenated at 300, 400, and 500 °C for 20 hours. Kinetic analysis, based on mass-variation data, reaction rates, and degree of conversion, reveals a multi-stage process involving surface-controlled reactions, diffusion-controlled growth, and equilibrium saturation. Arrhenius analysis indicates changes in the rate-controlling mechanism during hydrogen absorption. The tendency to reach the absorption equilibrium state was observed to occur more rapidly at 300°C, while the rate decreased as the temperature increased to 400°C and 500°C. Furthermore, it was found that higher temperatures led to greater absorption capacity. Overall, the titanium–hydrogen system exhibits complex, temperature-dependent kinetics, supporting its applicability in hydrogen storage technologies.*

Keywords: *hydrogen isotope storage; titanium hydride; metal hydrides; hydriding kinetics; thermogravimetry; Arrhenius analysis.*

1. INTRODUCTION

The identification of materials for hydrogen isotope storage that ensure high safety and efficiency is of major importance, particularly in nuclear fission and fusion energy research. These efforts are driven by the need to manage tritium generated during the operation of nuclear fission reactors, to ensure its storage, and to enable its subsequent use as a fuel in fusion reactors. In recent years, growing concerns about global warming and the urgent need for clean, sustainable energy sources have further increased interest in hydrogen and its storage. Hydrogen is considered a promising energy carrier because it does not

[1] RATEN Institute for Nuclear Research, Pitesti, Romania. E-mail: irina.paraschiv@nuclear.ro
[2] National University of Science and Technology POLITEHNICA Bucharest, Doctoral School of Materials Science and Engineering, Bucharest, Romania.

https://doi.org/10.46939/J.Sci.Arts-26.2-c01

contribute to atmospheric pollution and is not directly dependent on exhaustible fossil resources.

Three main methods for hydrogen storage are currently known: *(i)* gaseous storage (in pressurised tanks and cylinders), *(ii)* liquid storage (at cryogenic temperatures), and *(iii)* solid-state storage (via absorption or adsorption in various hydrogen-absorbing materials) [1-6]. Owing to its numerous advantages reported in the scientific literature [7-12] (relatively low operating pressures, high safety, the absence of evaporation losses, and high storage capacity), solid-state storage is considered the safest and most practical approach for hydrogen isotope storage and transportation.

Regarding this promising storage method, considerable research efforts focus on identifying materials that meet as many of the requirements for efficient hydrogen storage as possible [13-15], as shown in Fig. 1.

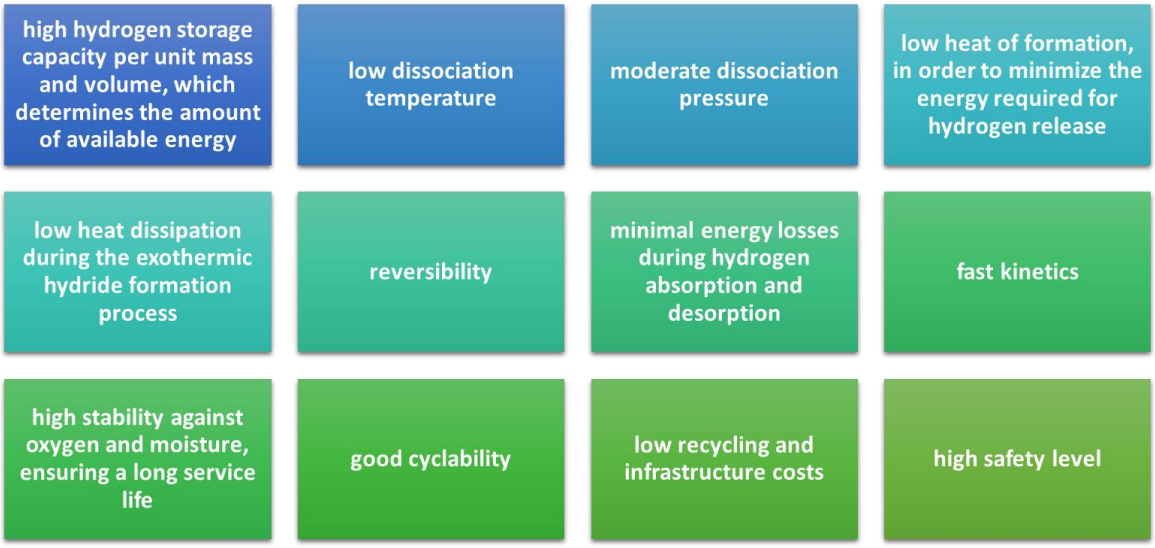

Figure 1. Requirements for hydrogen storage materials.

Metal hydrides are among the most promising classes of materials for hydrogen isotope storage applications. However, their practical application is strongly influenced by the kinetics of hydrogen absorption and desorption, which govern the material's hydriding and dehydring rates [16-18]. Therefore, a thorough understanding of these mechanisms is essential for the development of efficient and sustainable hydrogen isotope storage solutions. The study of the metal–hydrogen system provides valuable insight into the interaction between hydrogen and metals during hydride formation, as well as into the kinetic and thermodynamic mechanisms involved. Such knowledge is crucial for the development and optimization of materials for hydrogen storage, particularly in energy applications.

Understanding the fundamental concepts of hydrogen sorption in metals [19] is essential, as it provides the theoretical framework for interpreting absorption and desorption mechanisms. It explains how hydrogen interacts with metals, defines key sorption parameters, and facilitates interpretation of experimental results. Research on hydrogen absorption and desorption kinetics aims to understand the underlying molecular mechanisms and to identify factors that affect reaction rates, such as temperature, pressure, and material structure. Kinetic studies also enable the determination of key parameters [20], such as reaction rate constants and activation energies, providing essential information for optimizing material performance. Among the materials of interest, titanium and its alloys are particularly attractive due to their low density and high affinity for hydrogen, allowing the formation of metal hydrides.

Although numerous studies have reported the hydrogen absorption behaviour of titanium, differences in experimental conditions often lead to variations in the reported kinetic parameters and proposed reaction mechanisms. Therefore, further investigation is required to better understand the relationship between hydriding temperature, kinetic behaviour, and the mechanisms controlling hydrogen absorption.

Most studies have focused on phase formation, hydrogen storage capacity, thermodynamic behaviour, or the characterization of hydride phases. Comparative kinetic analyses combining thermogravimetric measurements, conversion-factor analysis, multiple solid-state kinetic models, and Arrhenius evaluation over a wide conversion range remain relatively limited. Therefore, the objective of the present paper is to investigate the hydriding behaviour of titanium in the Ti–H system at three different temperatures by correlating thermogravimetric data with kinetic modelling and Arrhenius analysis. This approach enables the identification of the dominant mechanisms governing the different stages of hydrogen absorption and provides a more comprehensive description of the hydriding process under the investigated conditions.

1.1. METAL – HYDROGEN INTERACTION

Metal hydrides are formed when transition metals react with hydrogen, typically in a reversible manner. The general reaction for hydride formation is given by Equation (1):

$$M + \frac{x}{2} H_2 \leftrightarrow MH_x + \Delta H \tag{1}$$

where M is the metal, x represents the stoichiometric ratio of hydrogen to metal, indicating how many hydrogen atoms are bonded to each metal atom, and ΔH is the enthalpy of hydride formation [21].

The formation of metal hydrides is a multistep process that proceeds through several stages and phase transformations before a hydride with a specific stoichiometry is obtained [21-28], as schematically illustrated in Fig. 2.

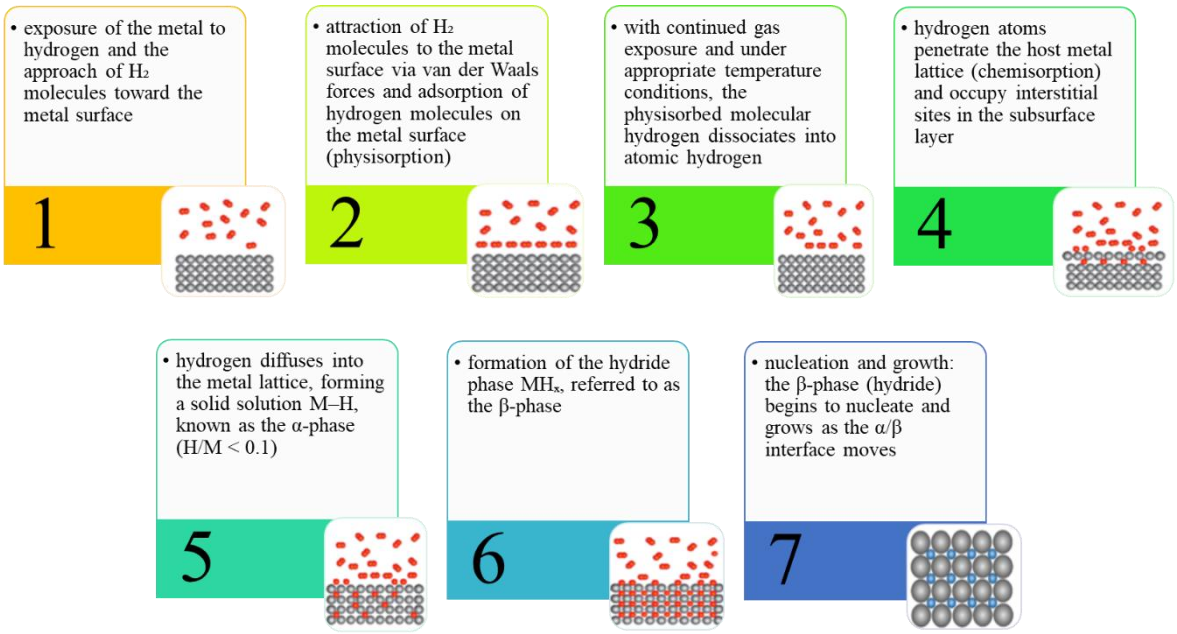

Figure 2. Metal hydride formation process.

In titanium, hydrogen absorption leads to the formation of different crystalline phases, depending on the absorbed hydrogen content, temperature, and pressure. To better understand the hydriding mechanism, the phase diagram of the titanium–hydrogen system is shown in Fig. 3 [29]. As observed, several allotropic forms are present, as reported in the scientific literature [30], including the α, β, δ, and ε phases, whose stability depends on hydrogen concentration, temperature, and pressure.

At low hydrogen concentrations, hydrogen forms interstitial solid solutions in the α–Ti (**hcp**) and β–Ti (**bcc**) phases, whereas at higher concentrations, hydride phases are formed. The solubility of hydrogen in α–Ti at room temperature is approximately 0.12 at.% H and increases with temperature, reaching a maximum value of 7.9 at.% (i.e., at.% is atomic percentage) at the eutectic temperature of 300 °C. This value remains approximately constant up to 600 °C, after which it decreases.

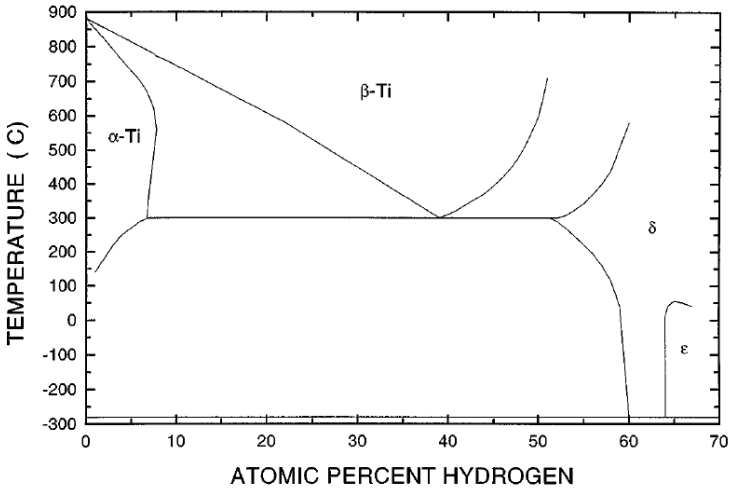

Figure 3. Ti – H phase diagram.
Source: image reproduced as is from [29].

At temperatures above 880 °C, pure titanium exhibits a body-centred cubic structure (β–Ti). The presence of dissolved hydrogen lowers the α-to-β phase transition temperature (β-transus), thereby acting as a β-phase stabiliser. The stable hydride phase with the lowest hydrogen concentration, the δ-phase, which has a face-centred cubic (**fcc**) structure of the CaF_2 type. This phase can coexist with α–δ or β–δ solid solution mixtures over a wide range of hydrogen compositions. At room temperature, it forms a single-phase material in the hydrogen concentration range of 60–66 at.% H, while this range becomes broader at elevated temperatures. The ε-phase, which is a tetragonally distorted **fcc** hydride with an axial ratio $c/a < 1$, forms at high hydrogen concentrations, where the atomic ratio H/Ti is approximately 2:1.

Finally, a metastable hydride precipitates within the α–Ti(H) solid solution, in which the hydrogen content ranges from 1 to 3 at.%. This hydride is referred to as the γ-phase and has a tetragonal structure with an axial ratio $c/a > 1$ [29, 31, 32].

1.2. KINETIC MEASUREMENT TECHNIQUES

The hydrogen absorption/desorption properties can be determined using various gas sorption measurement techniques, the principal ones being volumetric and gravimetric methods [34-38]: (i) the volumetric method is based on monitoring pressure variations within a calibrated volume; (ii) the gravimetric method relies on recording the change in mass of a sample subjected to a hydrogen absorption or desorption process. When the variation in the

mass of a sample is measured as a function of temperature, the thermogravimetric analysis (TGA) is used. In this paper, hydrogen sorption behaviour in titanium powder was analysed using the thermogravimetric method.

2. EXPERIMENTAL INVESTIGATION OF HYDROGEN ABSORPTION IN TITANIUM POWDER

2.1. MATERIALS AND EQUIPMENT

For the performed experiments, elemental Ti powder supplied by Alfa Aesar (Thermo Scientific, Waltham, US) was used. According to the manufacturer's certificate of analysis, the powder had a purity of 99.4% and a particle size of −100 mesh (~149 μm). The atmospheres used during the experiments were: *(i)* an inert atmosphere of argon with a purity of 99.999%; (ii) a hydriding atmosphere of hydrogen with a purity of 99.995%.

The experiments were performed using a SETARAM Setsys Evolution 24 thermoanalyzer (Setaram, Caluire-et-Cuire, France). The instrument operates at atmospheric pressure and temperatures up to 1400°C, and can be used under various gaseous atmospheres. The furnace is equipped with a microbalance capable of measuring masses from ±200 mg to ±2 g. Experimental programming and data acquisition were performed using the SETARAM Setsoft 2000 software (Setaram, Caluire-et-Cuire, France).

2.2. EXPERIMENTAL HYDRIDING METHOD

The first step in conducting the experiments consisted of weighing the titanium powders required for the study. To investigate hydrogen absorption at three temperatures, three Ti powder samples were prepared. The required quantities were determined by weighing using an analytical balance, with a precision of ±0.00001 g. Each sample was introduced individually into the thermoanalyser and processed according to the experimental program after initialization.

It should be noted that most materials are reactive and tend to form surface oxides that hinder hydrogen absorption; therefore, most metal hydrides require an activation step [37]. For the Ti powder, activation was performed by heating the sample from 25 °C to 800 °C (at a rate of 50 °C/min), holding it at 800 °C for 1 h, and then cooling it to the target hydriding temperature (at a rate of 20 °C/min). These steps were conducted under an argon (Ar) atmosphere. After activation, the hydriding stage was initiated by maintaining the samples at the target hydriding temperature for 20 h in a hydrogen atmosphere. Three hydriding temperatures were investigated in this study: 500 °C (sample 1), 400 °C (sample 2), and 300 °C (sample 3).

Investigating the hydrogenation kinetics at 300 °C, 400 °C, and 500 °C is relevant because hydrogen behaviour in titanium is strongly temperature-dependent, both thermodynamically and kinetically. At ~300 °C, the system is in the region where hydrogen solubility in the α–Ti phase reaches a maximum (approximately 7.9 at.% H), which corresponds to the eutectic temperature range. Under these conditions, the system approaches the stability limit of the solid solution, and hydride formation is strongly governed by the balance between dissolution and precipitation.

At higher temperatures (400 °C and 500 °C), hydrogen solubility in α–Ti does not increase significantly and even tends to decrease, while hydrogen diffusivity in the lattice increases substantially. This allows a clearer distinction between thermodynamic effects (phase stability and solubility) and kinetic effects (transport rate and hydride nucleation) [29, 31, 32].

Therefore, including 400 °C and 500 °C provides a comprehensive view of the transition from a solubility-controlled regime (near 300 °C) to a diffusion-controlled regime with accelerated transformation kinetics, enabling a more robust interpretation of the hydrogenation mechanism in titanium.

Under the experimental conditions, hydrogen uptake during the cooling stage is considered negligible; therefore, only the isothermal hydrogenation exposure contributes significantly to the kinetics of hydrogen absorption and hydride formation. This is why, after the 20-hour exposure to hydrogen, the working gas was switched to argon, and cooling was performed at a rate of 20 °C/min. Fig. 4 illustrates the experimental procedure.

Figure 4. Applied experimental methodology

This study focused only on data from the hydriding stage. The results were processed to determine mass variations, conversion factors, and reaction rates, thereby facilitating the analysis of kinetic rate constants and reaction mechanisms and the construction of the Arrhenius plot.

3. RESULTS AND DISCUSSION

3.1. MASS VARIATIONS DURING HYDRIDING AND THE CONVERSION FACTOR

Mass variations during the hydriding treatment illustrate the increase in sample mass as hydrogen is absorbed and are useful for identifying the point at which the mass becomes constant, indicating that the hydriding process has stabilized. From the experimental data, the final mass gain increases with hydriding temperature (as shown in Fig. 5a). Furthermore, with respect to the saturation tendency, a stabilization trend is observed (the curve approaches a plateau) after different time intervals depending on the temperature. Under the applied experimental conditions, higher hydriding temperatures required longer times for the samples to begin approaching saturation.

Recorded mass gains ranged from approximately 15 to 50 mg, allowing the estimation of the maximum hydrogen absorption capacity. While a significant difference in mass gain was observed between the samples hydrided at 300 °C and 400 °C, the difference between the samples hydrided at 400 °C and 500 °C was negligible.

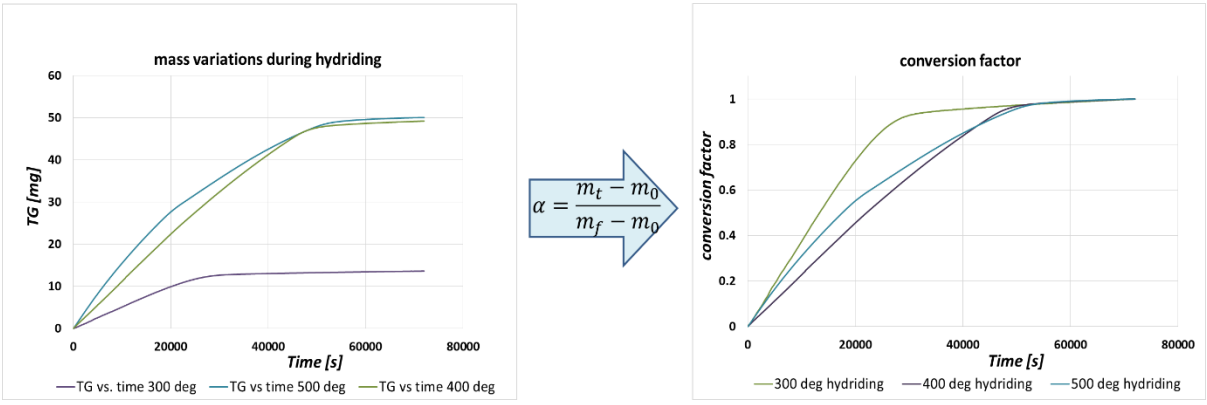

Figure 5. Mass variation and conversion factor.

To quantify the amount of hydrogen absorbed compared to the maximum theoretical capacity, the conversion factor (α), also referred to as the reaction fraction, is used. Since the experimental data did not allow a definitive conclusion on whether equilibrium was reached after 20 hours of hydriding, the conversion factor was adopted as a "relative parameter" for comparing the isothermally treated samples.

This coefficient is determined using Equation (2):

$$\alpha = \frac{m_t - m_0}{m_f - m_0} \tag{2}$$

where: m_t is the mass at time t, m_0 is the initial mass before absorption, and m_f is the final mass after absorption.

This parameter can only take values between 0 and 1 (α = 0 → no hydrogen absorbed; α = 1 → maximum saturation), thus enabling comparison of hydrogen absorption across different materials or experimental conditions.

Fig. 5b shows the variation of the conversion factor during the hydriding experiments. The results indicate different hydriding rates as a function of temperature. At 300 °C, the absorption process is the fastest, with α increasing more rapidly, indicating a shorter time required to reach the same hydrogen fraction. Compared to the samples hydrided at 400 °C and 500 °C, the absorption rate decreases with increasing temperature, while no significant differences are observed at 400 °C and 500 °C.

3.2. REACTION RATE VARIATION (dα/dt) AND THE RATE OF MASS CHANGE (dTG/dt)

As previously mentioned, the parameter α indicates the fraction of hydrogen absorbed at a given time. Its time derivative (dα/dt) represents the instantaneous hydrogen absorption rate and is an important parameter in the kinetic analysis of the process. Fig. 6 presents the corresponding experimental plots.

The analysis of the experimental reaction rate curves (dα/dt) highlights the evolution of the hydrogen absorption process, indicating regions where the reaction accelerates or decelerates, clearly distinguishing the initial, intermediate, and saturation stages.

The derivative curve (dTG/dt) represents the rate of mass change during the experiments and indicates how rapidly hydrogen is absorbed or desorbed at a given moment of the reaction. The rate of mass variation for the three experiments is also presented in Fig. 6.

The peaks in the dTG curve correspond to maximum rates of mass loss or gain and can be used to identify the kinetic regions for Arrhenius analysis or the application of reaction models. As expected, dα/dt and dTG/dt are proportional, although scaled differently.

The presence of multiple peaks in both the dα/dt and dTG/dt curves indicates that the process occurs in several stages. Consequently, the curves were divided into distinct regions, each of which was analyzed separately to determine rate constants and construct Arrhenius plots.

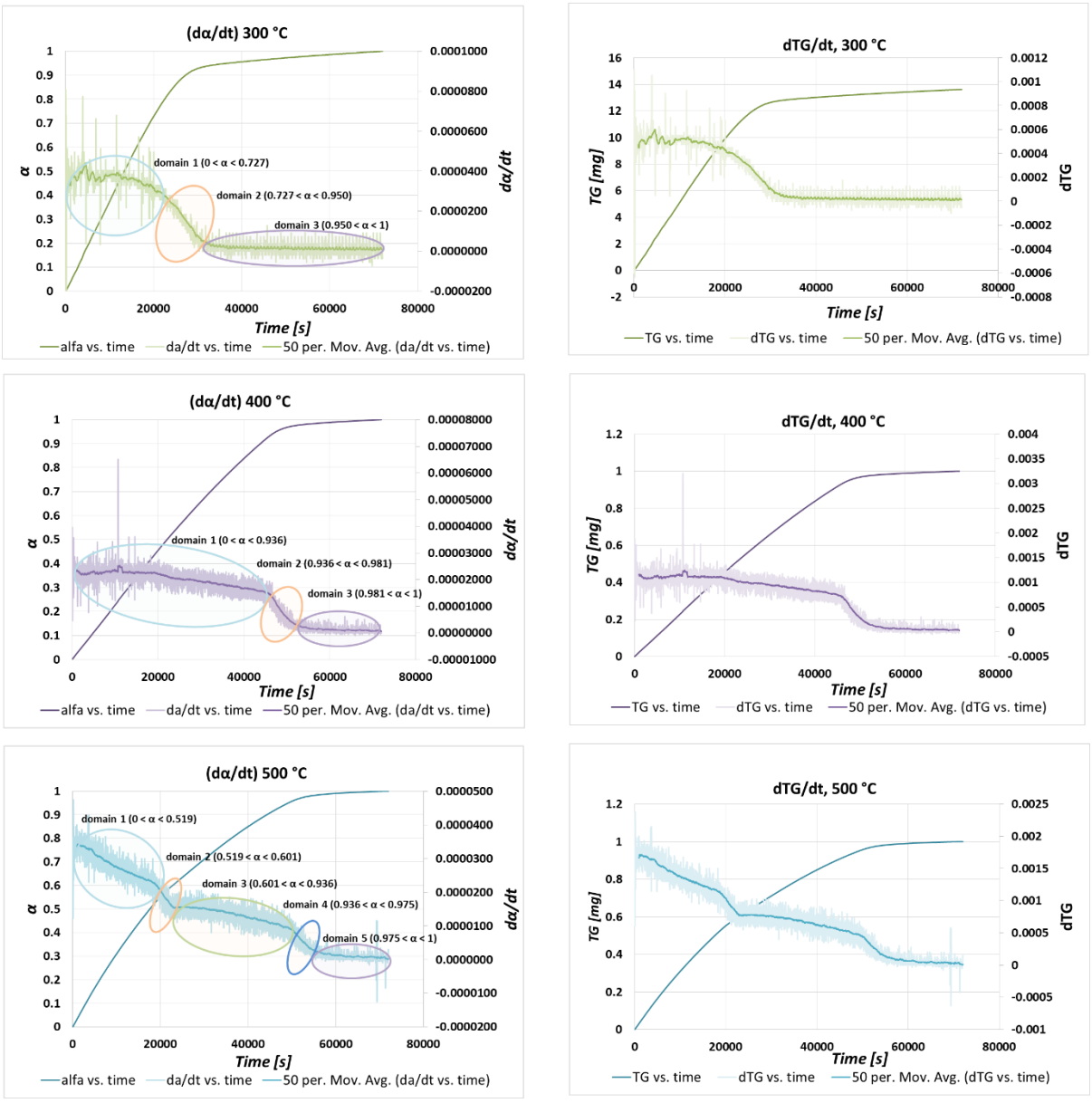

Figure 6. Reaction rate variation (dα/dt) and the rate of mass change (dTG/dt).

3.3. DETERMINATION OF THE KINETIC CONSTANT

To evaluate the kinetics of the titanium hydriding process, the rate constant, k, was determined by fitting the experimental data with various empirical models reported in the literature: simple zero-, first-, and second-order models, as well as physico-kinetic models commonly used for solid-state reactions (i.e., Jander, Ginstling–Brounshtein, Avrami,

Contracting Sphere). The equations corresponding to each model are presented in Table 1 [38].

Order-based models describe the dependence of the reaction rate on the conversion factor α and are primarily applicable to the initial stages of the reaction. The Avrami–Erofeev model is used for processes involving nucleation and growth of the product phase, providing information on the growth exponent and the kinetic constant.

Diffusion-controlled models (i.e., the Jander equation and the Ginstling–Brounshtein equation) and the Contracting Sphere model describe reaction stages in which the formation of a product layer limits the reaction rate. In these cases, the reaction is controlled either by diffusion through the product layer or by the progressive reduction of the reactive surface area.

The combined application of these models allows the identification of the dominant mechanisms across different conversion ranges and temperatures, providing a more complete description of the overall hydriding process.

Table 1. Kinetic models used in experimental study.

Type of model		**Integrated/linearized equation**	**Graphical representation**
Simple empirical models	0 - Order	$\alpha = kt$	α vs t
	1st - Order	$-\ln(1-\alpha) = 1 + kt$	-ln(1-α) vs t
	2nd -Order	$\frac{1}{1-\alpha} = 1 + kt$	1/(1-α) vs t
Physico-chemical models	Contracting sphere	$1-(1-\alpha)^{\frac{1}{3}} = kt$	$-(1-\alpha)^{\frac{1}{3}}$ vs t
	Jander	$g(\alpha) = 1 - \frac{3}{2}(1-\alpha)^{1/3} + \frac{1}{2}(1-\alpha) = kt$	g(α) vs t
	Ginstling - Brounshtein	$g(\alpha) = 1 - \frac{2\alpha}{3} - (1-\alpha)^{\frac{2}{3}} = kt$	g(α) vs t
	Avrami - Erofeev	$[-ln(1-\alpha)]^{1/n} = kt$	$ln[-ln(1-\alpha)]$ vs ln t

For each model, the experimental data were linearized using the corresponding equations (Table 1), and a linear fit was applied. The quality of the fit was evaluated using the correlation coefficient R^2, which reflects the agreement between the model and the experimental data.

The graphical analysis allowed the estimation of the rate constant k for each studied temperature and reaction domain, providing an initial evaluation of the apparent reaction rate and a basis for comparing potential transformation mechanisms. The kinetic rate constant k was determined from the slope of the linearized plots at each temperature.

3.3.1. Determination of the kinetic constant for the 300°C hydriding experiment

Following the application of the experimental data to the equation of each kinetic model presented in Table 1 (for each identified domain), different values of the correlation coefficient (R^2) were obtained.

For the experiments performed at 300 °C, the most appropriate models for each kinetic domain were selected based on the highest correlation coefficient ($R^2 \sim 1$). The rate constant was then determined from the slope of the corresponding linearized equations, and the results are presented in Table 2.

Table 2. Optimal kinetic models for describing the domains of Ti hydriding at 300 °C.

Domain	R^2	*Potential selected model*	*Equation*		*k*
1	0,9996	0 - Order	y = 4E-05x	✓	0.00004
2	0.9908	2nd - Order	y = 0.0011x - 20.501	✓	0.0011
3	0.993	Contracting core	y = 5E-07x + 0.9665	✓	0.0000001
	0.9937	0 - Order	y = 1E-06x + 0.9011	x	-

** The table presents only the models that best describe each kinetic domain*
*** The rate constants (k) were determined from the slopes of the linearized representations corresponding to each model*

The analysis of the titanium hydriding process at 300 °C reveals three distinct kinetic domains, corresponding to successive reaction mechanisms.

In domain 1 ($0 < \alpha < 0.727$), the process is best described by a zero-order model ($R^2 = 0.9996$), indicating a surface-controlled regime with an approximately constant reaction rate due to the easy accessibility of hydrogen.

In domain 2 ($0.727 < \alpha < 0.950$), the second-order model provides the best fit ($R^2 = 0.9908$), suggesting an interfacial mechanism in which the reaction rate depends on the concentration of reactive hydrogen and on the growth of the hydride phase at the metal–hydride interface.

In the final domain ($0.950 < \alpha < 1$), although the zero-order model gives a slightly better statistical fit ($R^2 = 0.9937$), the physical interpretation and the shape of the curve indicate that this stage is limited by hydrogen diffusion through the compact hydride layer. Therefore, the contracting core model ($R^2 = 0.990$) was selected based on physical considerations, indicating diffusion limitations as the TiH_2 layer thickens.

3.3.2. Determination of the kinetic constant for the 400°C hydriding experiment

Table 3 presents the best-fitting models for each domain in the hydriding experiments performed at 400 °C, selected based on the highest correlation coefficient (R^2).

Table 3. Optimal kinetic models for describing the domains of Ti hydriding at 400 °C.

Domain	R^2	*Potential selected model*	*Equation*		*k*
1	0.9942	0 - Order	y = 2E-05x	✓	0.00002
2	0.9989	2nd - Order	y = 0.0046x - 201.77	✓	0.0046
3	0.9916	0 - Order	y = 1E-06x + 0.925	x	-
	0.9915	Ginstling - Brounshtein	y = 3E-06x + 0.1103	✓	0.000003

** The table presents only the models that best describe each kinetic domain*
*** The rate constants (k) were determined from the slopes of the linearized representations corresponding to each model*

At 400 °C, three kinetic domains were identified.

In domain 1 ($0 < \alpha < 0.936$), the modelling indicated an excellent fit to a zero-order model ($R^2 = 0.9942$), suggesting a surface-reaction-controlled regime in which the reaction rate remains approximately constant.

In domain 2 ($0.936 < \alpha < 0.981$), the second-order model provides the best fit ($R^2 = 0.9989$), characteristic of a stage controlled by processes at the metal–hydride interface, where the propagation of the reaction front is dominant.

In the final domain ($0.981 < \alpha < 1$), similar correlation coefficients were obtained for the zero-order model ($R^2 = 0.9916$) and the Ginstling–Brounshtein model ($R^2 = 0.9915$), indicating a transition toward a diffusion-controlled regime. The Ginstling–Brounshtein model is selected based on physical considerations, as hydrogen diffusion through the TiH_x becomes rate-limiting.

3.3.3. Determination of the kinetic constant (k) for 500°C hydriding experiment

Table 4 presents the best-fitting models for each domain in the hydriding experiments performed at 500 °C, selected based on the highest correlation coefficient (R^2).

Table 4. Optimal kinetic models for describing the domains of Ti hydriding at 500 °C.

Domain	R^2	*Potential selected model*	*Equation*		*k*
1	0.9973	1st - Order	y = -4E-05x	✓	0.00004
2	0.9999	2nd - Order	y = 1E-04x - 0.6999	✓	0.0001
	0.9997	Jander	y = 7E-06x - 0.0594	x	-
	0.9995	Ginstling	y = 4E-06x - 0.0315	x	-
	0.999	1st - Order	y = -4E-05x + 0.0408	x	-
3	0.9907	Contracting core	y = 5E-06x + 0.7286	✓	0.000005
4	0.9996	1st - Order	y = -0.0002x + 6.2172	✓	0.0002
	0.9993	Jander	y = 3E-05x - 0.916	x	-
	0.9995	Avrami	y = 2.9375x - 30.634	x	-
5	0.9931	Ginstling	y = 3E-06x + 0.1008	✓	0.000003

** The table presents only the models that best describe each kinetic domain*
*** The rate constants (k) were determined from the slopes of the linearized representations corresponding to each model*

At 500 °C, five kinetic domains were identified.

In domain 1 ($0 < \alpha < 0.519$), the process follows a first-order model ($R^2 = 0.9973$), indicating that it is controlled by the adsorption and reaction of hydrogen at the metal surface.

In domain 2 ($0.519 < \alpha < 0.601$), the second-order model provides the best fit ($R^2 = 0.9973$), slightly exceeding diffusion models (i.e., Jander, Ginstling–Brounshtein equations). This stage may be attributed to the propagation of the metal–hydride interface, where the reaction rate is influenced by both the local availability of hydrogen and the effective surface area of the advancing TiH_x phase boundary. The fact that diffusion models also fit nearly as well suggests interfacial control with incipient diffusion limitations.

In domain 3 ($0.601 < \alpha < 0.936$), the Contracting Sphere model gives the best description ($R^2 = 0.9907$), indicating the progression of the reaction front toward the interior as the unreacted core shrinks.

In domain 4 ($0.936 < \alpha < 0.975$), the reaction temporarily returns to a first-order process ($R^2 = 0.9996$), likely due to the exposure of new internal surfaces. The fact that the Avrami model also provides an excellent fit ($R^2 = 0.9995$) suggests the simultaneous occurrence of nucleation and growth processes of the hydride phase.

For the final domain ($0.975 < \alpha < 1$), the Ginstling–Brounshtein model best describes the data ($R^2 = 0.9931$), indicating that the process enters a final stage controlled by hydrogen diffusion through the hydride layer.

To ensure the physical consistency of the kinetic parameters, only data from kinetically homologous domains should be included in the Arrhenius analysis. The identified homologous domains are summarized in Table 5. However, similarity between temperatures was observed only for two cases, which is insufficient to construct a reliable Arrhenius plot.

Table 5. Data needed for the Arrhenius plot.

Reaction stage	Kinetic model	Temperature [°C]	Rate constant, k [s^{-1}]
initial	1st - Order	500	0.00004
	0 - Order	400	0.00002
	0 - Order	300	0.00004
transitional	1st - Order	500	0.0002
	2nd - Order	400	0.0046
	2nd - Order	300	0.0011
final (saturation)	Ginstling	500	0.000003
	Ginstling	400	0.000003
	contr. core	300	0.0000005

Therefore, the kinetic coefficient (k) was also determined by considering the same α domains and fitting the experimental data using the Avrami model. The selection of this model was based on its versatility compared with classical kinetic models, as it can simultaneously describe nucleation and phase growth, providing a more realistic representation of complex structural transformations.

The data were linearized as ln[-ln(1-α)] vs ln t, and the fitting procedure yielded the corresponding equations and coefficients of determination (R^2), as presented in Table 6.

Table 6. Equations obtained from Avrami fitting.

α domain	300 °C		400 °C		500 °C	
	Equation	R^2	Equation	R^2	Equation	R^2
0 -1	y=1.2227x-11.878	0.9879	y=1.3679x-13.781	0.9689	y=1.2538x-12.463	0.9690
0 -0.3	y=1.1086x-11.018	0.9982	y=1.0219x-10.793	0.9974	y=1.0453x-10.618	0.9997
0.3-0.8	y=1.4732x-14.338	0.9971	y=1.4129x-14.484	0.9965	y=1.1190x-11.309	0.9991
0.8-1	y=0.9087x-8.4892	0.9381	y=1.9046x-19.505	0.9669	y=2.2896x-23.628	0.9876

From these equations, the kinetic coefficients (k) listed in Table 7 were calculated. The slope of the fitted line represents the Avrami exponent (n), while the kinetic coefficient k was derived from the intercept ($k = e^{-intercept}$, where e=2.718).

Table 7. Kinetic parameters (k) obtained using Avrami fitting.

Temperature	α domain							
	0<α<1		0<α<0.3		0.3<α<0.8		0.8<α<1	
	k	ln (k)	k	ln (k)	k	ln (k)	k	ln (k)
300	6.95E-06	-11.876	1.64E-05	-11.016	5.94E-07	-14.336	2.06E-04	-8.487
400	1.04E-06	-13.779	2.06E-05	-10.791	5.13E-07	-14.482	3.39E-09	-19.502
500	3.87E-06	-12.461	2.45E-05	-10.616	1.23E-05	-11.307	5.49E-11	-23.625

The kinetic rate constants obtained at each temperature enable analysis of the temperature–rate dependence using the Arrhenius relationship, thereby determining the activation energy and pre-exponential factor for the titanium hydriding process investigated in this study.

3.4. ARRHENIUS PLOT

The linear Arrhenius plot was used to evaluate the temperature dependence of the reaction rate constant and to determine the activation energy from the slope of the linear regression. The Arrhenius relationship, given by Equation (3), describes the dependence of the reaction rate constant on temperature:

$$k = Ae^{-\frac{E_a}{RT}} \tag{3}$$

where k is the reaction rate constant, A is the pre-exponential factor (or frequency factor), representing the probability of molecules colliding in a favorable orientation, E_a is the activation energy of the reaction (expressed in J/mol), R is the universal gas constant (8.314 J/mol·K), T is the absolute temperature (in K), and e is the base of the natural logarithm.

Using the activation energy and the pre-exponential factor, it is possible to predict both the reaction rate and the degree of conversion, α, at any temperature and reaction time without performing additional experiments.

The logarithmic form of the Arrhenius equation is Equation (4). This expression can be written in the linear form given by Equation (5), which is used to construct the Arrhenius plots:

$$\ln k = \ln A - \frac{E_a}{R} \cdot \frac{1}{T} \tag{4}$$

$$\ln k = -\frac{E_a}{R} \cdot \frac{1}{T} + \ln A \tag{5}$$

Using Equation (5), an Arrhenius plot of ln k *vs.* 1/T was constructed (Fig. 7). Temperatures were converted from degrees Celsius to Kelvin using the relationship T [K] = 273.15 + T °C.

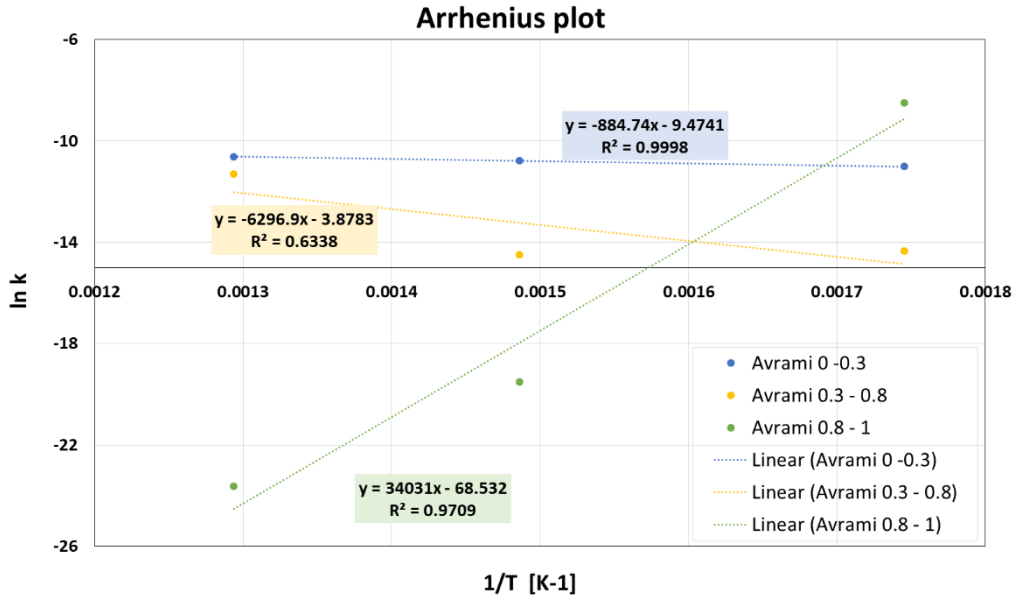

Figure 7. Arrhenius plot for Ti hydriding kinetics, at 300 °C, 400 °C and 500 °C

3.4.1. Determination of activation energy

The activation energy, E_a, represents the minimum energy required for the reaction to occur and reflects the sensitivity of the reaction rate to temperature variations.

From the slope of the Arrhenius plot, the activation energy E_a can be determined using Equation (6) and Equation (7):

$$slope = -\frac{E_a}{R} \tag{6}$$

$$E_a = -slope \cdot R \tag{7}$$

As observed from the plot shown in Fig. 7, the obtained linearized equations were:

- for $0<\alpha<0.3$: $y = -884.74x - 9.4741$;
- for $0.3<\alpha<0.8$: $y = -6296.9x - 3.8783$;
- for $0.8<\alpha<1$: $y = 34031x - 68.532$.

Using the gas constant ($R = 8.31$ J/mol·K), and applying Equation (7), the activation energies corresponding to the three conversion intervals were determined as follows (using 1 kJ/mol = 1000 J/mol unit conversion:

- for $0<\alpha<0.3$: $E_a = 7.35$ kJ/mol;
- for $0.3<\alpha<0.8$: $E_a = 52.32$ kJ/mol;
- for $0.8<\alpha<1$: $E_a = -282.79$ kJ/mol.

3.4.2. Determination of the pre-exponential factor

The pre-exponential factor, A, represents the frequency of effective collisions between reactant species and provides information regarding the probability of successful reaction events. The reaction rate constant at any temperature can be calculated using Equation (8):

$$k = A \cdot e^{-E_a/(RT)} \tag{8}$$

In general, a high A value indicates a large number of effective molecular collisions and kinetically favourable conditions, whereas a low A value suggests that the reaction is more strongly influenced by geometrical or configurational constraints.

The pre-exponential factor is obtained from the intercept of the Arrhenius plot using Equation (9) and Equation (10):

$$\ln A = intercept \tag{9}$$

$$A = e^{intercept} \tag{10}$$

Using the intercept values obtained from the linear regressions shown in Fig. 7, the pre-exponential factors were calculated as follows:

- for $0<\alpha<0.3$: $A = 7.68 \times 10^{-5}$;
- for $0.3<\alpha<0.8$: $A = 2.07 \times 10^{-2}$;
- for $0.8<\alpha<1$: $A = 1.73 \times 10^{-30}$.

The analysis indicates that hydrogen absorption in titanium cannot be described by a single kinetic mechanism over the entire conversion range investigated. For the intervals $0<\alpha<0.3$ and $0.3<\alpha<0.8$, the relatively low activation energy indicates a weak temperature dependence of the reaction rate.

In the $0.8<\alpha<1$ domain, the system approaches a saturated state as hydride layers progressively develop around the titanium particles. These layers hinder hydrogen transport toward the remaining unreacted titanium core, resulting in increasing diffusion limitations. The positive slope observed for this conversion interval results in an apparent negative activation energy. Such a value should not be interpreted as a true physical activation barrier but rather as evidence that the Avrami model is no longer adequate for describing the reaction kinetics in this stage. Similar behaviour has been reported in studies where diffusion through hydride layers and mass-transfer limitations become the dominant rate-controlling mechanisms. It should also be noted that the activation energies were determined using a limited number of experimental temperatures; therefore, the associated uncertainty may be significant.

4. CONCLUSIONS

Metal hydrides are among the most promising materials for hydrogen storage because they offer enhanced safety compared with conventional storage methods and exhibit high volumetric hydrogen density. However, their practical application is strongly influenced by the kinetics of hydrogen absorption and desorption, which govern the rates of hydriding and dehydriding in the material. The study of metal–hydrogen systems provides insight into the mechanisms governing hydride formation and decomposition. A thorough understanding of these processes is essential for evaluating the performance of hydrogen storage materials and assessing their suitability for specific applications. Among the candidate materials, Ti (and its alloys) are particularly attractive due to their low density, high affinity for hydrogen, and ability to form metal hydrides reversibly.

This paper presents a comparative kinetic analysis of hydrogen absorption in titanium (a promising candidate material for hydrogen storage) under different experimental conditions. Although the kinetic models are well-established and widely used in the literature, the novelty of the present paper lies in their comparative application to the investigated system under the selected experimental conditions. By evaluating the suitability of various kinetic models and analysing the resulting kinetic parameters, this study provides further insight into the mechanisms governing the process under investigation.

The main contribution of this study is the comparative kinetic assessment of titanium hydriding using thermogravimetric measurements, conversion-factor analysis, kinetic modelling, and Arrhenius analysis. The results demonstrate that distinct kinetic mechanisms dominate at different conversion intervals, confirming the multi-stage nature of the hydriding process under the experimental conditions investigated.

The observations derived from the experiments and subsequent kinetic data analysis can be summarised as follows: (i) Increasing the hydriding temperature prolongs the time required to reach saturation. Differences in the final absorption capacity become noticeable only at 300 °C and 400 °C. At 500 °C, the mass gain reaches a plateau, indicating the approach to a hydriding limit and a stronger influence of diffusion and microstructural effects during the final stages of the reaction. *(ii)* Analysis of the conversion factor shows that Ti hydriding proceeds most rapidly at 300 °C, where α increases faster and the hydrogen uptake time is reduced. At 400 °C and 500 °C, the absorption rate decreases slightly, with only minor differences between the two temperatures, suggesting that lower temperatures within this interval are more favourable for hydrogen absorption. *(iii)* The experimental reaction rate curves ($d\alpha/dt$) obtained at different temperatures reveal the evolution of the hydrogen absorption process. The shape of the $d\alpha/dt$ vs α curve served as the basis for selecting kinetic

models that describe the dominant reaction. *(iv)* The occurrence of multiple peaks in both dα/dt and dTG/dt curves indicates that hydrogen absorption proceeds through several stages. Consequently, the curves were divided into distinct regions and analyzed separately to identify the appropriate kinetic models for each stage. *(v)* The determination of kinetic coefficients and activation energies confirmed the complex nature of the hydrogenation process. The results demonstrate that no single kinetic model can adequately describe the entire reaction pathway under the investigated conditions. *(vi)* Overall, the observed behaviour is consistent with a nucleation–growth–saturation mechanism that is characteristic of metal hydride formation.

REFERENCES

[1] Seemita, B., *Studies on advanced materials for hydrogen storage*, Homi Bhabha National Institute, Mumbai, 2013 (a thesis submitted to the Board of Studies in Chemical Sciences for the Degree of Doctor of Philosophy).

[2] Osman, A. I., Ayati, A., Farrokhi, M., Khadempir, S., Rajabzadeh, A. R., Farghali, M., Krivoshapkin, P., Tanhaei, B., Rooney, D. W., Yap, P.S., Innovations in hydrogen storage materials: Synthesis, applications, and prospects, *J. Energy Storage*, **95**, 112376, 2024.

[3] Liu, H., Zhang, J., Sun, P., Zhou, C., Liu, Y., Fang, Z. Z., An overview of TiFe alloys for hydrogen storage: Structure, processes, properties, and applications, *J. Energy Storage*, **68**, 107772, 2023.

[4] Salehabadi, A., Dawi, E. A., Sabur, D. A., Al-Azzawi, W. K., Salavati-Niasari, M., Progress on nano-scaled alloys and mixed metal oxides in solid-state hydrogen storage; an overview, *J. Energy Storage*, **61**, 106722, 2023.

[5] Demirocak, D. E., *Hydrogen Storage Technologies*. In Chen, Y.-P.et al. (Eds.), *Nanostructured materials for next-generation energy storage and conversion*, Springer-Verlag GmbH, Germany, 2017, https://doi.org/10.1007/978-3-662-53514-1_4.

[6] Hirscher, M., Eds., *Handbook of hydrogen storage: new materials for future energy storage*, John Wiley & Sons, Germany, 2010.

[7] Motyka, T., *Hydrides for processing and storing tritium*, in Proceedings of *50 Years of Excellence in Science and Engineering at the Savannah River Site*, Savannah River Site (US), United States, 2000. https://www.osti.gov/biblio/754224

[8] Fraunhofer Institute for Manufacturing Technology and Advanced Materials IFAM, *Hydrides for H_2 Storage*, [Online]. Available: https://www.ifam.fraunhofer.de/en/Aboutus/Locations/Dresden/HydrogenTechnology/hydrides/hydrides-for-h2-storage.html. (Accessed 16 04 2025).

[9] Walker, G., *Solid-state hydrogen storage: materials and chemistry*, Woodhead Publishing, Cambridge, 2008.

[10] Klopcic, N., Grimmer, I., Winkler, F., Sartory, M., Trattner, A., A review on metal hydride materials for hydrogen storage, *J. Energy Storage*, **72**, 108456, 2023, https://doi.org/10.1016/j.est.2023.108456.

[11] Li, J., Advancements in metal hydride materials for hydrogen storage, *Highlight Sci Eng Technol.*, **58**, 313, 2023

[12] Liu, Y., Chabane, D., Elkedim, O., Intermetallic compounds synthesized by mechanical alloying for solid-state hydrogen storage: A review, *Energies*, **14**, 5758, 2021, https://doi.org/10.3390/en14185758

[13] https://energy.gov/eere/fuelcells/downloads/doe-targets-onboard-hydrogen-storage-systems-light-duty-vehicles
[14] Sujan, G. K., Pan, Z., Li, H., Liang, D., Alam, N., An overview on TiFe intermetallic for solid-state hydrogen storage: microstructure, hydrogenation and fabrication processes, *Critical Reviews in Solid State and Materials Sciences*, **45**, 410, 2020,
[15] Balat, M., Potential importance of hydrogen as a future solution to environmental and transportation problems, *Int. J. Hydrog. Energy*, **33**, 4013-4029, 2008.
[16] Puszkiel, J. A., *Tailoring the kinetic behavior of hydride forming materials for hydrogen storage*. In Rahman, M. M., Asiri, A. M. A., (Eds.), *Gold nanoparticles - Reaching new heights*, IntechOpen, United Kingdom, 2019, http://dx.doi.org/10.5772/intechopen.82433
[17] Abd. Khalim Khafidz, N. Z., Yaakob, Z., Lim, K. L., Timmiati, S. N., The kinetics of lightweight solid-state hydrogen storage materials: A review, *Int. J. Hydrog. Energy.*, 2016, http://dx.doi.org/10.1016/j.ijhydene.2016.05.169
[18] Yang, J. Sudik, A., Wolverton, C., Siegel, D. J., High-capacity hydrogen storage materials: attributes for automotive applications and techniques for materials discovery, *Chem. Soc. Rev*.,**39**, 656–675, 2010, https://doi.org/10.1039/b802882f
[19] Gross, K. J., Carrington, K. R., *Recommended best practices for the characterization of storage properties of hydrogen storage materials*, U.S. Department of Energy (DOE) / National Renewable Energy Laboratory (NREL), Washington, D.C, 2008
[20] Broom, D. P., *Hydrogen storage materials - The characterisation of their storage properties*, Springer Science & Business Media, London, 2011, https://doi.org/10.1007/978-0-85729-221-6
[21] Shashikala, K., *Hydrogen storage materials*, in Banerjee, S., Tyagi, A. K., (Eds.), *Functional materials – Preparation, processing and applications*, Springer Cham, Switzerland, 2019.
[22] Kumar, S., *Studies on hydrogen interaction with vanadium and vanadium-aluminium alloys, Homi Bhabha National Institute, Mumbai*, 2012, (A thesis submitted to the Board of Studies in Chemical Sciences Discipline for the Degree of Doctor of Philosophy).
[23] Abe, J. O., Popoola, A. P. I., Ajenifuja, E., Popoola, O. M., Hydrogen energy, economy and storage: Review and recommendation, *Int. J. Hydrog. Energy*, **44**, 15072, 2019, https://doi.org/10.1016/j.ijhydene.2019.04.068
[24] Drawer, C., Lange, J., Kaltschmitt, M., Metal hydrides for hydrogen storage – Identification and evaluation of stationary and transportation applications, *J. Energy Storage*, **77**, 109988, 2024, https://doi.org/10.1016/j.est.2023.109988.
[25] Shelyapina, M. G., *Metal hydrides for energy storage*, In: Martínez, L., Kharissova, O., Kharisov, B. (Eds.), *Handbook of ecomaterials*, Springer, Cham, 775-810, 2019, https://doi.org/10.1007/978-3-319-68255-6_119
[26] Lototskyy, M. V., Tarasov, B. P., Yartys, V. A., Gas-phase applications of metal hydrides, *J. Energy Storage*, **73**,108165, 2023.
[27] Züttel, A., Materials for hydrogen storage, *Materials Today*, **6**, 24-33, 2003, https://doi.org/10.1016/S1369-7021(03)00922-2)
[28] Sakintuna, B., Lamaridarkrim, F., Hirscher, M., Metal hydride materials for solid hydrogen storage: A review, *Int. J. Hydrog. Energy*, **32**, 1121, 2007.
[29] Checchetto, R., Scardi, P., Structural characterization of deuterated titanium thin films, *Journal of Materials Research*, **14**, 1969, 1999, https://doi.org/10.1557/JMR.1999.0265
[30] Numakura, H., Koiwa, M., Hydride precipitation in titanium, *Acta Metallurgica*, **32**, 1799, 1984

[31] Sandim, H. R. Z., Morante, B. V., Suzuki, P. A., Kinetics of thermal decomposition of titanium hydride powder using in situ high-temperature X-ray diffraction (HTXRD), *Materials Research*, **8**, 293, 2005, https://doi.org/10.1590/S1516-14392005000300012
[32] Straumal, B. B., Kilmametov, A.R., Ivanisenko, Yu., Mazilkin, A.A., Valiev, R.Z., Afonikova, N.S., Gornakova, A.S., Hahn, H., Diffusive and displacive phase transitions in Ti–Fe and Ti–Co alloys under high pressure torsion, *Journal of Alloys and Compounds*, **735**, 2281, 2018, https://doi.org/10.1016/j.jallcom.2017.11.317
[33] Huot, J., *Kinetics and Thermodynamics*. In A. Léon (Ed.), *Hydrogen Technology: Mobile and Portable Applications*, Berlin, Heidelberg: Springer, 471, 2008, https://doi.org/10.1007/978-3-540-69925-5_19
[34] Friedlmeier, G., Schaaf, M., Groll, M., How to Measure Pressure-Concentration-Isotherms Representative for Technical Applications, *Zeitschrift für Physikalische Chemie*, **183**, 185, 1994, https://doi.org/10.1524/zpch.1994.183.Part_1_2.185
[35] Poirier, E., Chahine, R., Tessier, A., Bose, T. K., Gravimetric and volumetric approaches adapted for hydrogen sorption measurements with in situ conditioning on small sorbent samples, *Rev. Sci. Instrum.*, **76**, 055101, 2005, https://doi.org/10.1063/1.1891647
[36] Brown, M. E., *Introduction to Thermal Analysis: Techniques and Applications (2nd edition)*, Springer Science & Business Media, 2001.
[37] Bednarova, L., Brestovic, T., Jasminska, N., Lazar, M., Dobakova, R., Toth, L., The impact of metal hydride material activation on the storage percentage of hydrogen in this material, *IJIER*, **8**, 25, 2020, https://doi.org/10.31686/ijier.Vol8.Iss01.194
[38] Koradia, V., de Diego, H.L., Elema, M.R. and Rantanen, J., Integrated approach to study the dehydration kinetics of nitrofurantoin monohydrate. *J. Pharm. Sci.*, **99**, 3966, 2010, https://doi.org/10.1002/jps.22244